Fault detection and isolation for Polymer Electrolyte Membrane Fuel Cell systems by analyzing cell voltage generated space

CrossMark

Zhongliang Li [a,b,c,*], Rachid Outbib [b], Stefan Giurgea [a,c], Daniel Hissel [a,c], Yongdong Li [d]

[a] FCLAB (Fuel Cell Lab) Research Federation, FR CNRS 3539, rue Thierry Mieg, 90010 Belfort Cedex, France
[b] Laboratoire des Sciences de l'Information et des Systemes (LSIS), University of Aix-Marseille, France
[c] FEMTO-ST (UMR CNRS 6174), ENERGY Department, University of Franche-Comte, France
[d] Department of Electrical Engineering, Tsinghua University, Beijing 100084, China

HIGHLIGHTS

- A novel data-driven fault diagnosis approach for Polymer Electrolyte Membrane Fuel Cell (PEMFC) systems is proposed.
- Experiments in different failure modes are emulated over two different PEMFC stacks.
- Multiple faults can be detected and isolated with high accuracy.
- Only low-cost voltage sensors are used.
- Computing burden is light to realize the online implementation.

ARTICLE INFO

ABSTRACT

This paper proposes a data-driven diagnostic approach for Polymer Electrolyte Membrane Fuel Cell (PEMFC) systems. Fault detection and isolation (FDI) is realized by analyzing individual cell voltages. A feature extraction method *Fisher Discriminant Analysis* (FDA) and a multi-class classification method *Directed Acyclic Graph Support Vector Machine* (DAGSVM) are utilized successively to extract the useful features from raw data and classify the extracted features into various classes related to health states. Experimental data of two different stacks are used to validate the proposed approach. The results show that five concerned faults can be detected and isolated with a high accuracy. Moreover, the light computational cost of the approach enhances the possibility of its online implementation.

© 2015 Elsevier Ltd. All rights reserved.

1. Introduction

Increasing environment and resource issues are motivating the development and commercialization of fuel cell technologies. Polymer Electrolyte Membrane Fuel Cell (PEMFC) is one of the most promising fuel cells, especially for automotive applications. Although considerable effort has been devoted to advancing the PEMFC technologies, and significant progress has been achieved over the last decades, some challenges still need to be overcome.

For the fuel cell system itself, cost and durability are always two key barriers [1].

On the one hand, the cost of manufacturing needs to be further lowered. The current (projected high-volume manufacturing) cost announced in 2012 has been lowered to $47 kW^{-1} [2]. It is still higher than the target value of $30 kW^{-1}, which is considered as a competitive value in the mainstream transportation sector. On the other hand, to achieve large scale market penetration, durability is another technical hurdle. For instance, the lifetime of no less than 40,000 h for stationary applications and 5000 h for electric vehicles is the target in the strategic Plan of the U.S. Department of Energy (DOE) [3]. Substantial progress has been made in lengthening the lifetime of fuel cells, and the highest demonstrated durability of stationary and automotive fuel cells can currently reach to 20,000 h and 2500 h respectively [4]. However, the distance to target is still great.

To minimize the fuel cell performance degradation, much effort is being made on the research on degradation mechanisms of materials, and the design and assembly of fuel cells. Apart from these internal improvements, making PEMFC and the stack operate in an optimal condition can certainly mitigate the performance degradation. Fault diagnosis, considered as a crucial component of PEMFC system operation management, is currently receiving considerably increasing attention. Through efficient diagnosis, more serious faults can be avoided thanks to an early fault alarm. Based on the diagnostic results, operating conditions can be adjusted to make the fuel cell operate efficiently and safely. Moreover, the precise diagnosis information can speed up the development of new technologies and reduce the downtime (repair time) [5]. Actually, fault diagnosis is playing an increasingly important role in some kinds of modern industrial systems [6–8]. However, to the authors' knowledge, the development of the diagnosis approach for fuel cell systems is still comparatively lagging behind the other development areas in fuel cell technology.

Studies conducted recently can provide some diagnosis solutions. Model-based (analytical model) diagnosis is an intuitional way to realize the aim of fault detection and isolation (FDI) [9,10]. If a proper model is available, a number of standard methods could be available for the FDI design [11]. However, the identification of fuel cell inner parameters is usually difficult to achieve, which makes accurate modeling a PEMFC stack a hard or even impossible task [12]. Besides, some accurate models, such as multi-dimensional ones, require considerable processing time, and are thus not always suitable for diagnosis in real-time [9].

To overcome the drawbacks of model based approaches, some data-driven methods have also been proposed for PEMFC diagnosis [13–16]. Thanks to the contributions from the computer science and information community in the last decade, the data-driven fault diagnosis has merged a large amount of electronic and computer technology, such as some pattern recognition and artificial intelligent methods as well as some signal processing methods. With the advantages and experiences of these methods, data-driven fault diagnosis seems to be a promising direction for PEMFC systems.

Although a number of data-driven fault diagnosis designs have been proposed, more efforts still need to be taken on this topic. First, in some proposals, some special measurements and/or experiments, such as electrochemical impedance spectroscopy (EIS), rather than the regular measurements are used for diagnosis [17]. In order to reduce the cost and avoid additional disturbance, the variables used for diagnosis should be measured with minimal instrumentation and even without any additional instrumentation. Second, the available approaches mainly focus on the capability of the detection of some specific faults, especially the faults in fuel cells. Much less attention is paid to the aspect of fault isolation which is another main element of fault diagnosis. To make the diagnosis procedure more completed and efficient, fault isolation should be attached more importance. To do this, amount of experiments under different faulty operation conditions should be carried out and investigated. Third, for practical real-time applications, diagnosis accuracy and computational cost of the diagnosis algorithm are two crucial criteria, which should be evaluated in depth.

This paper is dedicated to the design of a new data-driven PEMFC system diagnostic approach. Originally, the proposed approach belongs to the pattern classification domain. Specifically, individual cell voltages are employed here as the original variables for diagnosis. The approach, which is a two-stage procedure, is carried out in the cell voltage generated space. First, a feature extraction method FDA is used to get the features from raw data. After that, a multi-class classification method, named DAGSVM, is adopted to classify the features into various classes,

which represent the health states (fault free state and different faulty states) of the PEMFC system. FDI can thus be realized through this two-stage procedure.

The contributions of this study are summarized as follows:

- Only individual cell voltages are selected as the variables for diagnosis. Additional instrumentation is not needed in this case.
- Five faults that may occur in the different parts of PEMFC systems were emulated in the experiments. To demonstrate that the proposed approach is a robust diagnostic tool, experiments were carried out over two different PEMFC stacks (an 8-cell stack and a 40-cell stack). Concerning the five faults, both fault detection and fault isolation performances are evaluated.
- Diagnosis accuracy and computational cost of the proposed algorithm are validated to be suitable for online diagnosis.

The rest of the paper is organized as follows: In Section 2, the investigated stacks, test benches and experiments are presented. In Section 3, the methodologies used are expounded. After that, Section 4 is devoted to introducing the implementation of the diagnostic approach in detail. Following that, the diagnostic results and some discussion are given in Section 5. Finally, the conclusion and future work are summarized in Section 6.

2. Experimental investigations

2.1. Description of the PEMFC stacks

An 8-cell stack and a 40-cell stack were used to carry out various experimental tests, including the ones under fault conditions. The two stacks were fabricated by the French research organization CEA (Alternative Energies and Atomic Energy Commission) in the framework of the French ANR DIAPASON project. Both stacks have the same technology parameters except the number of cells. The nominal operating conditions of the two stacks are summarized in Table 1.

2.2. Description of the test benches

A 1 kW and a 10 kW test benches, which had been developed in-lab, were employed respectively to fulfill the experimental requirements of two PEMFC stacks. Fig. 1 shows the overall view of the 1 kW test bench (similar picture of 10 kW test bench can be found in [18]).

Both test benches can be divided into several subsystems:

- Air supply subsystem: The flow rate, pressure, temperature and hygrometry level at the air inlet can be regulated to the required conditions.
- Hydrogen supply subsystem: The flow rate and pressure at the hydrogen inlet, temperature and hygrometry level at the hydrogen inlet can be regulated to the required conditions.
- Temperature subsystem: This subsystem is dedicated to the control of stack temperature.
- Electronic load: The load current can be flexibly varied through an electronic load.
- Control/supervision unit: The controls of the test bench and the parameter monitoring are fulfilled using National Instruments Materials and Labview software. The variables that can be measured or monitored are summarized in Table 2.

The control of the humidifying of reactant gases is realized through regulation of the dew point temperatures of the upstream humidifiers. The test benches are equipped with cooling water circuits that enable the control of the stack temperatures. The

Table 1
Nominal conditions of the stacks.

Parameter	Value
Stoichiometry H_2	1.5
Stoichiometry Air	2
Pressure at H_2 inlet	150 kPa
Pressure at Air inlet	150 kPa
Differential of anode pressure and cathode pressure	30 kPa
Temperature (exit of cooling circuit)	80 °C
Anode relative humidity	50%
Cathode relative humidity	50%
Current	110 A
Voltage per cell	0.7 V
Electrical power of 8-cell stack	616 W
Electrical power of 40-cell stack	3080 W
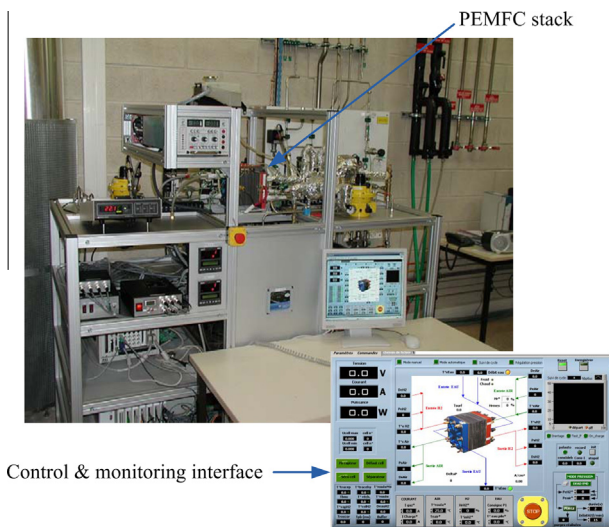
Fig. 1. Photograph of the 1 kW testbench.

Table 2
Measured variables.

Variable	Notation
Flow rate at the H_2 inlet	D_{in,H_2}
Pressure at the H_2 inlet	P_{in,H_2}
Pressure at the H_2 outlet	P_{out,H_2}
Temperature at the H_2 inlet	T_{in,H_2}
Temperature at the H_2 outlet	T_{out,H_2}
Relative humidity at the H_2 outlet	RH_{in,H_2}
Flow rate at the air inlet	$D_{in,air}$
Pressure at the air inlet	$P_{in,air}$
Pressure at the air outlet	$P_{out,air}$
Temperature at the air inlet	$T_{in,air}$
Temperature at the air outlet	$T_{out,air}$
Relative humidity at the air outlet	$RH_{in,air}$
Temperature at the cooling water inlet	$T_{in,water}$
Temperature at the cooling water outlet	$T_{out,water}$
Current	I
Stack voltage	V_s
nth cell voltage (from anode side)	v_n

temperature measured at the cooling water circuit outlet is considered as the stack temperature. More details about the two test benches can be found respectively in [19,20].

2.3. Experiments presentation

Experiments on the 8-cell stack and 40-cell stack were carried out in the 1 kW and 10 kW test benches respectively. In this study,

Table 3
Various concerned states.

Health state description	Location of state	Notation
Nominal operating state	Whole system	Nl
High current pulse or short circuit	Electric circuit	F_1
Stop cooling water	Temperature subsystem	F_2
High air stoichiometry	Air supply subsystem	F_3
Low air stoichiometry	Air supply subsystem	F_4
CO poisoning	H_2 supply subsystem	F_5

five faulty states other than fault free operating state were concerned. As Table 3 shows, the faults, caused by the abnormal operations of the electric circuit, temperature subsystem, air supply subsystem and hydrogen supply subsystem, were taken into consideration. In fact, the failures of the auxiliary subsystems usually result in the abnormal or non-optimal operations suffered by the stack. The faults studied are usually considered as "reversible" or "recoverable", which can be corrected through appropriate operations. The efficient FDI of such kind of faults is the key focus of the paper.

In order to obtain the datasets for both training and test aims, experiments were carried out several times in each condition.

3. Presentation of the methodologies for diagnosis

3.1. Framework of the diagnosis approach

The proposed diagnosis approach combines FDA (see for instance [21,22]) and DAGSVM methods. Fig. 2 outlines the framework of the diagnosis approach. As the figure shows, it contains the off-line training stage and on-line performing stage.

In the off-line training process, the training samples in the training dataset are distributed in various classes that represent health states, including the fault free state and a number of concerned fault states. The labeled samples are used to train the feature extraction method FDA and the classification method DAGSVM successively. The trained FDA and DAGSVM models are then prepared for on-line performing use.

In the on-line performing process, with the aid of the obtained FDA model, the features of real-time data are firstly extracted. DAGSVM is then carried out to classify the extracted features into a certain class and complete the diagnosis procedure.
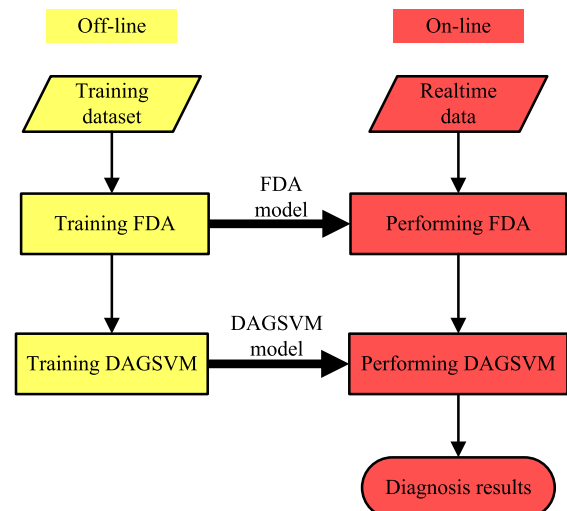
Fig. 2. Flowchart of the proposed diagnosis approach.

3.2. Mathematical description of FDA and DAGSVM

The diagnostic problem can be mathematically abstracted as follows. Suppose that we have a training dataset of NH-dimensional samples $\{\boldsymbol{x}_n \mid n \in \{1, \ldots, N\}\}$, which are distributed in C classes denoted by $\Omega_1, \Omega_2, \ldots, \Omega_C$. The cardinal (i.e. the number of the elements in Ω) of a set Ω is denoted as $|\Omega|$. FDA and DAGSVM models are trained based on the training dataset. Through the trained models, a real-time sample $\boldsymbol{x}$ can be classified into a defined class Ω_i, $i = 1, \ldots, C$.

FDA is a technique developed for feature extraction or dimension reduction in the hope of obtaining a more manageable classification problem. Through FDA, the original H-dimensional samples are projected onto an L-dimensional space, where $L \leqslant C - 1$ is usually the case [21]. The principle of FDA can be abstracted as Algorithm 1.

Algorithm 1. FDA

Training:
1: Collect $\boldsymbol{x}_1, \boldsymbol{x}_2, \ldots, \boldsymbol{x}_N$.
2: Calculate *within-class-scatter matrix* $\boldsymbol{S}_w$ and *between-class-scatter matrix* $\boldsymbol{S}_b$.

$$\boldsymbol{S}_w = \sum_{i=1}^{C} \sum_{\boldsymbol{x}_n \in \Omega_i} (\boldsymbol{x}_n - \bar{\boldsymbol{x}}_i)(\boldsymbol{x}_n - \bar{\boldsymbol{x}}_i)^T$$

$$\boldsymbol{S}_b = \sum_{i=1}^{C} |\Omega_i| (\bar{\boldsymbol{x}}_i - \bar{\boldsymbol{x}})(\bar{\boldsymbol{x}}_i - \bar{\boldsymbol{x}})^T$$

where $\bar{\boldsymbol{x}} = \sum_{n=1}^{N} \boldsymbol{x}_n/N$, and $\bar{\boldsymbol{x}}_i = \sum_{\boldsymbol{x}_n \in \Omega_i} \boldsymbol{x}_n / |\Omega_i|$.
3: Set $L \in \mathbb{N}, L \leqslant C - 1$. Find the L eigenvectors of $\boldsymbol{S}_w^{-1} \boldsymbol{S}_b : \boldsymbol{w}_1, \ldots, \boldsymbol{w}_L$, with eigenvalues $\lambda_1 \geqslant \ldots \geqslant \lambda_L$.
Performing:
Calculate the L features of a new sample $\boldsymbol{x}$ using projecting vectors $\boldsymbol{w}_1, \ldots, \boldsymbol{w}_L$:

$$\boldsymbol{z} = [\boldsymbol{w}_1^T \boldsymbol{x}, \boldsymbol{w}_2^T \boldsymbol{x}, \ldots, \boldsymbol{w}_L^T \boldsymbol{x}]^T \qquad (1)$$

By performing FDA to the training data as (1), the H-dimensional data can be projected to L-dimensional feature space as

$$\boldsymbol{z}_n = [\boldsymbol{w}_1^T \boldsymbol{x}_n, \boldsymbol{w}_2^T \boldsymbol{x}_n, \ldots, \boldsymbol{w}_L^T \boldsymbol{x}_n]^T \quad n = 1, \ldots, N \qquad (2)$$

DAGSVM is then carried out in the feature space. DAGSVM is a type of multi-class Support Vector Machine (SVM). The remarkable classification characteristics, such as good generalization performance, the absence of local minima and the sparse representation of solution, make SVM an attractive pattern classification tool [23].

DAGSVM is realized by solving a number of binary SVMs. Without deducing details (found in [24]), the binary SVM corresponding to the first two classes for instance can be summarized as Algorithm 2.

Algorithm 2. Binary SVM

Training:
1: Set D, σ.
2: Collect $z_1, z_2, \ldots, z_{|\Omega_1|+|\Omega_2|}$.
3: Solve the quadratic problem (QP):

$$\min J(\boldsymbol{a}) = \frac{1}{2} \sum_{n=1}^{|\Omega_1|+|\Omega_2|} \sum_{m=1}^{|\Omega_1|+|\Omega_2|} a_n a_m g_n g_m k(\boldsymbol{z}_n, \boldsymbol{z}_m) - \sum_{n=1}^{|\Omega_1|+|\Omega_2|} a_n$$

$$\text{s.t.} \sum_{n=1}^{|\Omega_1|+|\Omega_2|} a_n g_n = 0, \quad 0 \leqslant a_n \leqslant D \quad \text{for} \quad n = 1, 2, \ldots, |\Omega_1| + |\Omega_2|$$

$$(3)$$

with $g_n(\boldsymbol{z}) = 1$ if $\boldsymbol{z} \in \Omega_1$ and $g_n(\boldsymbol{z}) = -1$ if $\boldsymbol{z} \in \Omega_2$.
Where $\boldsymbol{a} = [a_1, a_2, \ldots, a_{|\Omega_1|+|\Omega_2|}]^T$ are the Lagrange multipliers, and

$$k(\boldsymbol{z}_n, \boldsymbol{z}_m) = exp\left(-\frac{||\boldsymbol{z}_n - \boldsymbol{z}_m||^2}{\sigma}\right) \qquad (4)$$

4: Save support vectors $\boldsymbol{z}_1^s, \boldsymbol{z}_2^s, \ldots, \boldsymbol{z}_S^s$ and corresponding g_n and a_n (denoted by $\{g_n^s\}$ and $\{a_n^s\}$) for which $a_n > 0$.
Performing:
For a new sample $\boldsymbol{z}$,

$$g(\boldsymbol{z}) = sign\left\{ \sum_{n=1}^{S} a_n^s g_n^s k(\boldsymbol{z}_n^s, \boldsymbol{z}) + \frac{1}{S} \sum_{j=1}^{S} \left(g_j^s - \sum_{n=1}^{S} a_n^s g_n^s k(\boldsymbol{z}_n^s, \boldsymbol{z}_j^s) \right) \right\} \qquad (5)$$

As presented in [25], to solve a C-class classification problem, it is necessary to construct all possible binary classifiers from a training set of classes, each classifier being trained on only two out of C classes. There would thus be $C(C - 1)/2$ classifiers. In the performing phase, a rooted binary directed acyclic graph (DAG), which has C layers, $C(C - 1)/2$ internal nodes and C leaves, is used. As Fig. 3 shows, each node is a binary SVM of ith and jth classes. Given a test sample, starting at the root node, the binary classification function at a node is evaluated. Then it moves to the node in the next layer from either left or right path (depending on the binary classification result). Then, the binary classification function of the next node is evaluated. Therefore, a path is taken before reaching a leaf node which indicates the predicted class. The path is known as the evaluation path which goes through $C - 1$ nodes. Carrying out $C - 1$ times of binary classifications is needed to derive the final class determination.

3.3. Remarks on the methodologies

1. It should be noted that there are other methods for feature extraction and classification than FDA and DAGSVM in the pattern classification domain. In our previously published article [26], some representative feature extraction and classification methods are compared from the perspectives of diagnosis accuracy and computational cost. FDA and SVM have shown outstanding performance in the two aspects.
2. It should be emphasized that although it seems to be sophisticated to address the training of the FDA and SVM models (the eigenvalue problem and QP problem for instance), the performing procedures of the trained models are much less burdened. Fortunately, for the practical on-line diagnosis, only the performing procedure is concerned.
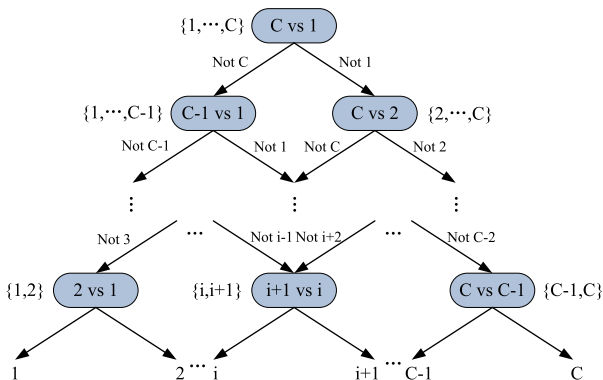

Fig. 3. DAGSVM structure.

(a) Stack voltage and current of 8-cell stack

(b) Stack voltage and current of 40-cell stack

(c) Temperatures and relative humidities of 8-cell stack

(d) Temperatures and relative humidities of 40-cell stack

(e) Pressures and flow rates of 8-cell stack
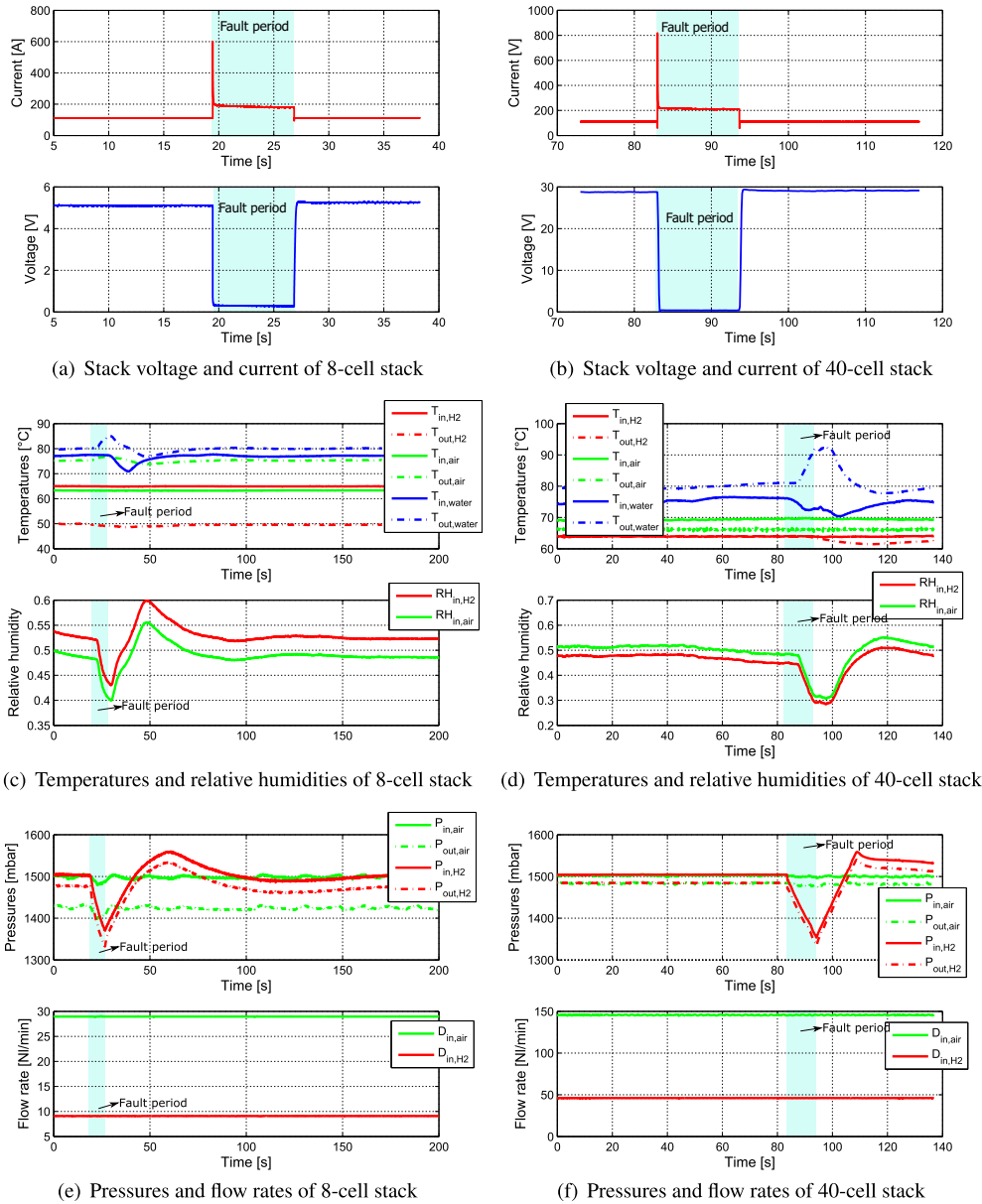
(f) Pressures and flow rates of 40-cell stack

Fig. 4. Measurements in F_1 process.

4. Application for PEMFC system diagnosis

4.1. Preliminary analysis of each fault

- High current pulse or short circuit (F_1)
  In the faulty experiments, high current pulse or short circuit was imposed between the two electrodes of the fuel cell stacks. Fig. 4(a) and (b) show the electrical behavior of the stack in a short circuit process. It can be seen that a current impact appeared at the beginning of the short circuit. The current then decreased to stabilize at a fixed value (near 2 times the nominal value). Here the current was limited by the mass transfer losses and by the hydrogen flow [27]. Fig. 4(c) and (d) show the temperatures and humidities of the two stacks in the F_1 process. The short circuit occurred from 19 s to 27 s for the 8-cell stack, and from 83 s to 94 s for the 40-cell stack approximately. The high current pulse in the process caused a rise in the stack temperature (reflected by the temperature at the outlet of cooling water).
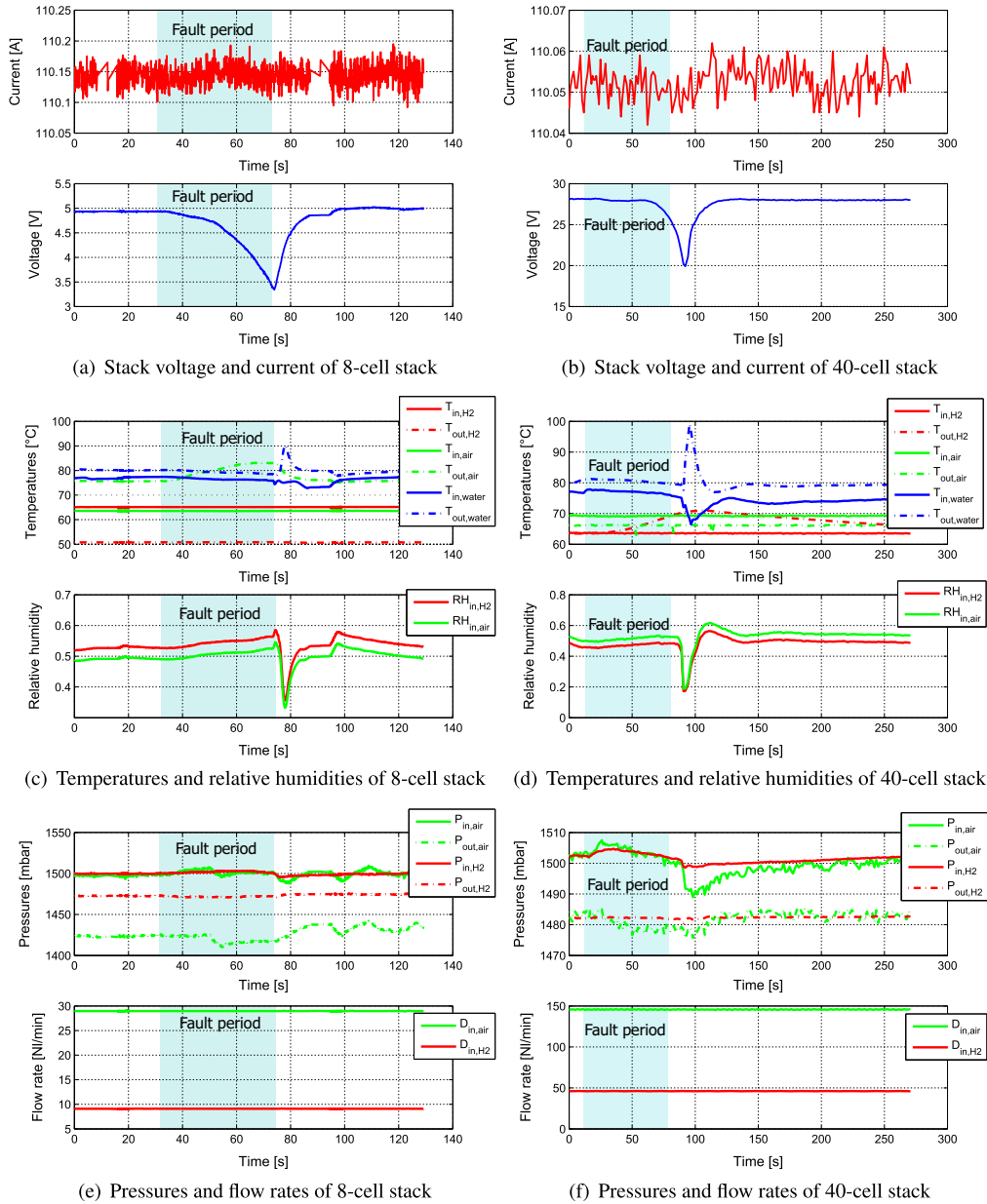
The temperature control unit functioned to decrease the stack temperature to the reference value. This is realized by decreasing $T_{in,water}$. The stack temperature was brought down with the help of the cooling circuit after the short circuit was eliminated. Since the saturation pressure of the fuel cell increased with the increasing of stack temperature, the relative humidities showed the inverted evolution of the stack temperature.

The pressures and gas flow rates in the process are shown in Fig. 4(e) and (f). It can be observed that the cathode pressure varied little, while the anode pressure decreased with the abrupt consumption of the hydrogen in the fault process. After the fault was eliminated, the anode pressure was recovered thanks to a pressure regulator. The flow rates of the gases did not vary basically.

- Stop cooling water (F_2)
  The F_2 fault was caused by stopping the cooling water for some time. Fig. 5 shows the experimental measurements in the F_2 process. The disconnection of the cooling water

(a) Stack voltage and current of 8-cell stack

(b) Stack voltage and current of 40-cell stack

(c) Temperatures and relative humidities of 8-cell stack

(d) Temperatures and relative humidities of 40-cell stack

(e) Pressures and flow rates of 8-cell stack

(f) Pressures and flow rates of 40-cell stack

Fig. 5. Measurements in F_2 process.

circuit occurred from 33 s to 76 s for the 8-cell stack, and from 8 s to 86 s for the 40-cell stack approximately.

Fig. 5(a) and (b) show the electrical behavior of the stack in the process. With the constant current, the stack voltage decreased in this period. After that, the cooling water circuit was reconnected and the stack voltage rose up to the nominal value with the function of temperature regulation. It should be noticed that no marked decrease in the voltage was observed in the first phase (from 8 s to about 60 s, decreased about 0.25 V). A fast decline happened from 60 s to 92 s (decreased about 8 V). For the 8-cell stack, voltage started decreasing when the cooling circuit was disconnected. The drops in the stack voltages could be connected to the membrane drying phenomenon. Actually, excessive temperature due to ineffective cooling can cause membrane dehydration and thus lower the conductivity of the membrane.

Temperatures and relative humidities in this process are shown in Fig. 5(c) and (d). For the 8-cell stack, the temperatures of hydrogen inlet and outlet, inlet of air, inlet and outlet

of cooling water showed little variation, while the temperature of air outlet increased in the process. For the 40-cell stack, the temperature at hydrogen outlet rose (from about 35 s to 100 s), while other temperatures showed no evident variations. Based on this observation, it is the reasonable to say that $T_{out,air}$ of the 8-cell stack and $T_{out,H2}$ of the 40-cell stack can better reflect the temperature variation of the stack than $T_{out,water}$ in the F_2 fault process. After the water circuit was reconnected, the $T_{out,water}$ was increased firstly under the influence of the internal temperature of the stack. Then, it decreased by regulation of the temperature subsystem. Concerning the relative humidities, an inverted evolution of $T_{out,water}$ could be observed for the humidities of both stacks. Fig. 5(e) and (f) show the pressures and flow rates in the F_2 fault process. It can be said that there were no evident variations on these variables during the experiment.

- High air stoichiometry (F_3) and low air stoichiometry (F_4)
  In the experiments of F_3 (F_4), air stoichiometry was set to values that are higher (lower) than the nominal value. The

(a) Stack voltage and current of 8-cell stack

(b) Stack voltage and current of 40-cell stack

(c) Temperatures and relative humidities of 8-cell stack

(d) Temperatures and relative humidities of 40-cell stack

(e) Pressures and flow rates of 8-cell stack

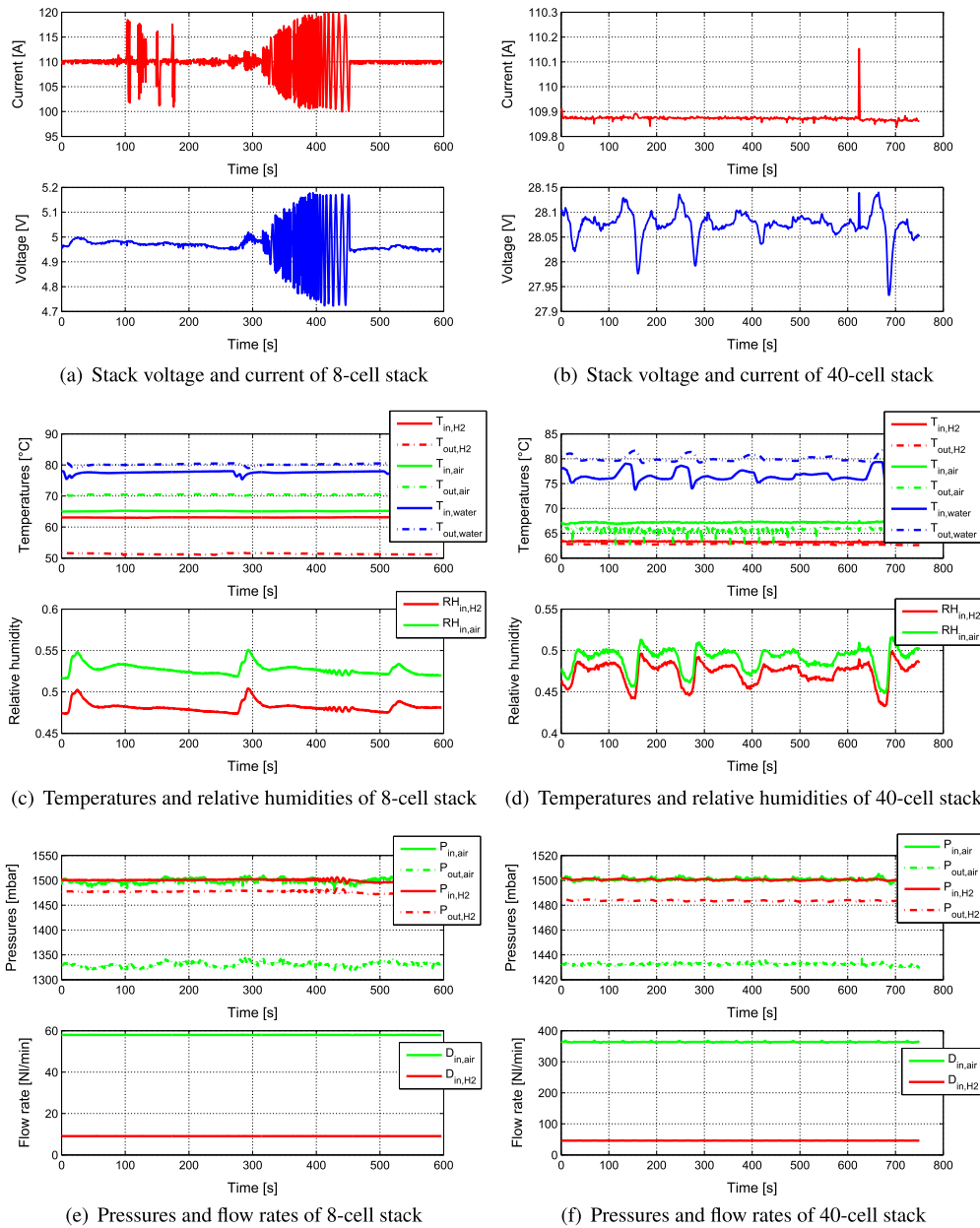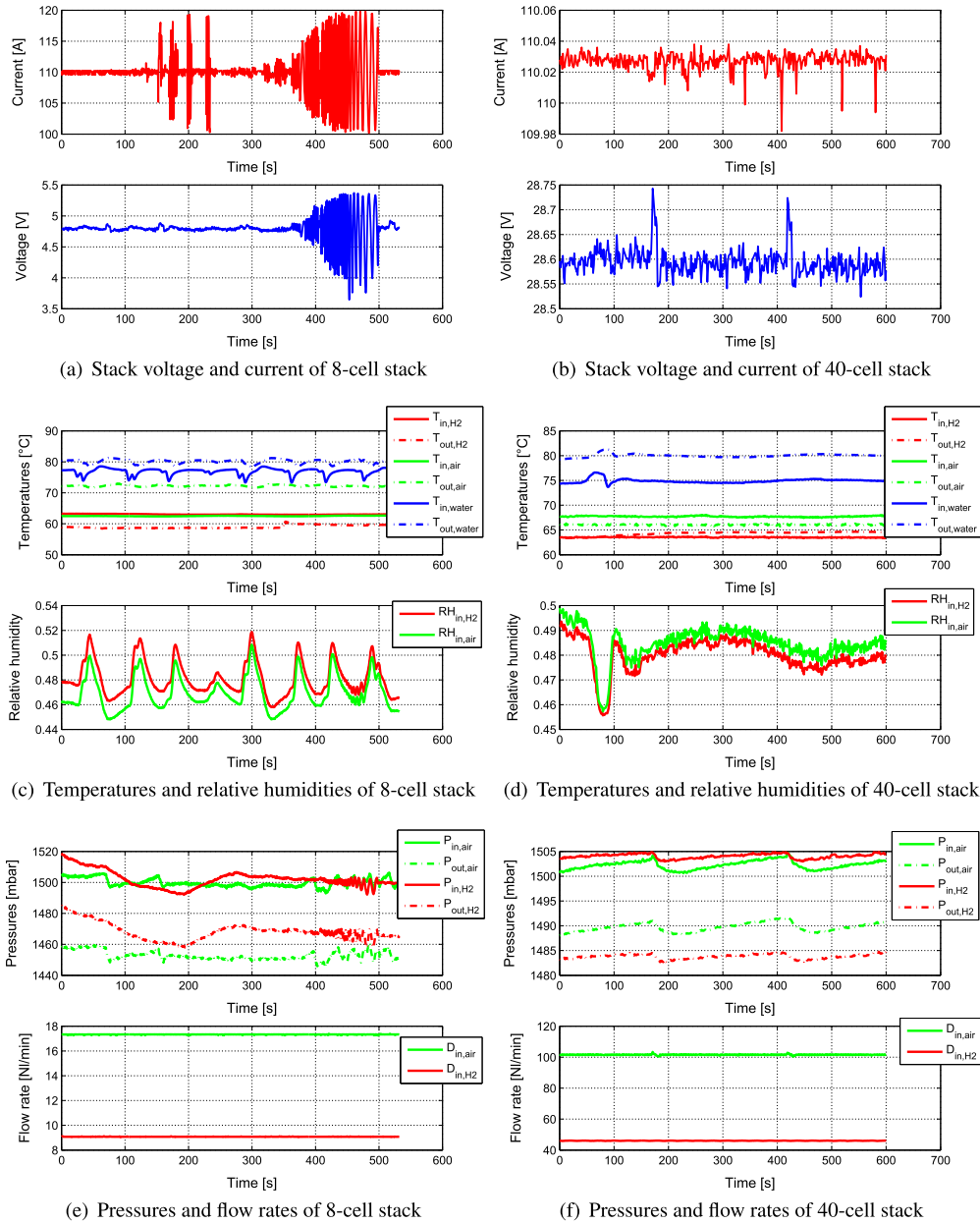(f) Pressures and flow rates of 40-cell stack

Fig. 6. Measurements in F_3 process.

difference between the set values and normal value are obviously bigger than the magnitude of noise. This means that the control objective of stoichiometry is not achieved. Some faults may happen in the air supply subsystem (for instance, air compressor and/or control algorithm). Actually, a fuel cell can operate within a range of air stoichiometry values without the appearance of severe degradation. The two cases should therefore be considered as faults of fuel cell system than the ones of fuel cells.

The electrical, thermal, and fluidic variables in a F_3 fault experiment are shown in Fig. 6. The air stoichiometry was set respectively at 4 for the 8-cell stack and 5 for the 40-cell stack. From the experimental results, it can be seen that the stack reached to a stable state. The temperatures of gases and cooling water did not markedly vary in the process. $P_{in,air}$ was maintained to be the nominal value, while $P_{out,air}$ was smaller compared to the value in a normal operating process. In fact, the difference in the pressures at the air

inlet and air outlet corresponds to the air flow rate. A larger flow rate usually results in a larger pressure difference [28]. With the nominal load, the stack voltages varied little from the nominal values. Note that during the F_3 and F_4 processes, electrochemical impedance spectra (EIS) tests were also carried out for the 8-cell stack. Some light-magnitude signals of various frequencies could be seen for both currents and stack voltages.

The electrical, thermal, and fluidic variables in the F_4 fault experiment are shown in Fig. 7. The air stoichiometry was set at 1.2 for the 8-cell stack and 1.4 for the 40-cell stack. As in the case of F_3, it can be seen that the stack reached to a stable state. The temperatures of various positions did not show obvious variations in the process. The pressure at the air inlet was maintained at the nominal value, while the pressure at the air outlet reached to a higher value, which was contrary to the case of F_3. Little variations are seen in the currents and stack voltages.

(a) Stack voltage and current of 8-cell stack

(b) Stack voltage and current of 40-cell stack

(c) Temperatures and relative humidities of 8-cell stack

(d) Temperatures and relative humidities of 40-cell stack

(e) Pressures and flow rates of 8-cell stack

(f) Pressures and flow rates of 40-cell stack

Fig. 7. Measurements in F_4 process.

Although the obvious degradation of fuel cell stacks did not appear during the F_3 and F_4 faults, these faults should be avoided in the long term run. On the one hand, low air stoichiometry could be an incentive factor that leads to cathode water flooding and cathode starvation. Both phenomena have been considered as the severe faults that can lead to very sharp degradation or even damage to the stack. On the other hand, an excessively high oxygen flow could result in membrane drying, decreasing the conductivity of the membrane. In addition, more power is consumed to get a higher air stoichiometry, which will lower the overall system efficiency [29].

• CO poisoning (F_5)

CO poisoning has been considered one of the most common faults for PEMFC. The presence of carbon monoxide can block or limit the active sites of the platinum catalyst, and thus decrease the fuel cell performance [30]. The experiment of fault F_5 was carried out by feeding the hydrogen with 10 ppm CO for 1.5 h (only on the 8-cell stack), and then

pure hydrogen was supplied instead of poisoned gas. In the process, EIS tests were performed several times.

The measurements are shown in Fig. 8. From a global point of view, the output stack voltage gradually decreased in the fault process and increased in the recovery process. The change rate of stack voltage decreased in both stages. The temperatures at the hydrogen outlet increased at the beginning of the fault process (to 1100 s approximately), and then decreased. The temperature rise could be correlated to the increase in the anodic impedance [30]. From Fig. 8(c), the pressure waves at the hydrogen inlet and outlet correspond to the current waveform, while the pressures at the air inlet and outlet varied little in the process.

Based on the above preliminary analysis, the faults concerned include the severe faults, which could cause the rapid degradation of the system performance, such as F_1, F_2, F_5, and the slight faults, such as F_3, F_4. It is observed that different faults result in the

(a) Stack voltage and current of 8-cell stack

(b) Temperatures and relative humidities of 8-cell stack
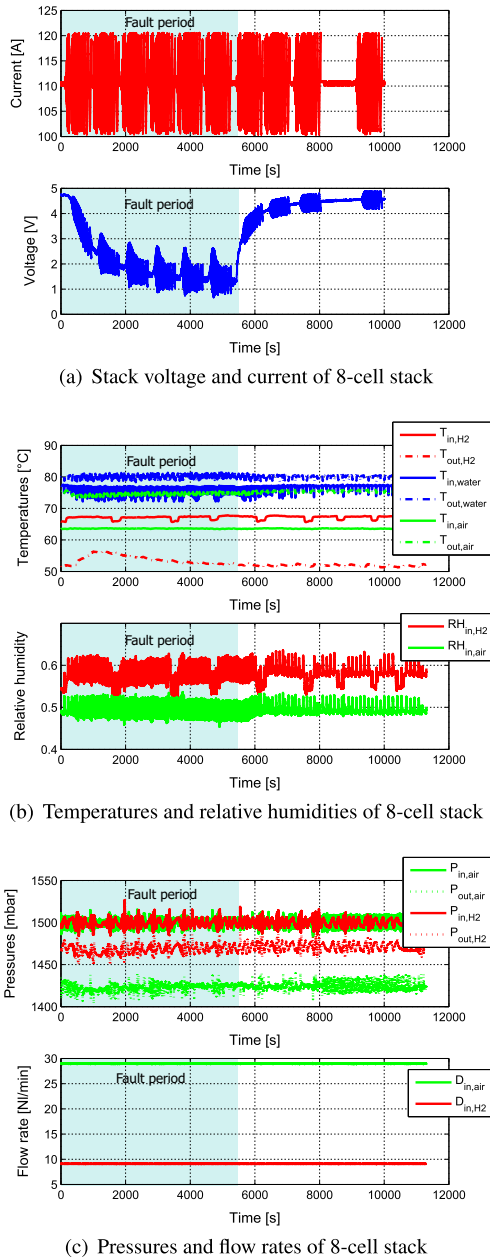

(c) Pressures and flow rates of 8-cell stack

Fig. 8. Measurements in F_5 process.

different variations of the measurements. From a practical perspective, the on-board instrumentation has to be minimized, and using a minimal number of low-cost sensors is usually desirable. In order to realize FDI of these faults, stack voltage is usually considered as an efficient variable since it is the output of the system (if the load current is seen as an input variable). However, only stack voltage seems to be feeble to achieve fault isolation aim. Fig. 9 shows the evolution of the cell voltages in the aforementioned processes. It could be found that the individual cell voltages are distributed more evenly in certain states (Nl, F_3, F_4) than that in others (F_1, F_2, F_5). Moreover, the spacial distribution of individual cell voltages varies with the type of fault. Essentially, different faults can lead to different spatial distributions of temperature, humidity, and gas fluids and thus result in the different spatial distributions of individual cell voltages. Without doubt, the individual cell voltages can supply more information for diagnosis than mere stack voltages. Hence, the individual cell voltages were chosen as the original variables for FDI in this study.

4.2. Implementations of the diagnostic approach

When the fault free dataset and the datasets of the concerned faults are available in hand, the fault diagnosis can be considered as a classification problem. For the 8-cell stack, the class number is 6 (including the classes of Nl, F_1, F_2, F_3, F_4, F_5), while the one for the 40-cell stack is 5 (including the classes of Nl, F_1, F_2, F_3, F_4). At each time point, the vector composed by individual cell voltages is considered as the original variable for diagnosis. So 8-dimensional data and 40-dimensional data are processed respectively for the 8-cell stack and the 40-cell stack.

To implement and verify the approach, the datasets for training and test should firstly be prepared. As both FDA and SVM methods are supervised ones, the samples in different classes must be prepared and labeled to construct the datasets for training and test. For states Nl, F_3, and F_4, the corresponding experiments were carried out in constant conditions. The data sampled during the experiments can be labeled with the corresponding class labels arbitrarily. Differently, in the experiments of F_2, F_3 and F_5, the faults occurred in between the normal operating states. The samples in the faulty operating time intervals were collected. Since several experiments were done for each condition, the samples in one (or several) specific experiment(s) were employed as the training data, while the samples from other experiments were collected as test data. The sample numbers in different classes for training and testing are shown in Table 4. Notice that, in order to cover the fault zones, the dataset with longer duration is usually selected for training. Hence, the test data is less than training data for some classes (F_2 of 40-cell stack).

4.2.1. FDA procedure

In this procedure, the cell voltage composed vectors are projected into the low-dimensional feature space by using FDA. In the FDA operation, the dimension of the projected space must be less than the number of classes (see Section 3). The maximum feature space dimension number is therefore 5 for the 8-cell stack and 4 for the 40-cell stack.

Through the training process, 5 projecting vectors are obtained for the 8-cell stack, while the number of the projecting vectors is 4 for the 40-cell stack. The eigenvalues can reflect the amount of discriminant information that the corresponding projecting vectors can preserve. To indicate the proportion of the eigenvalues corresponding to the projecting vectors in all non-zero eigenvalues, the accumulation contribution rate (ACR) is defined:

$$ACR = \frac{\sum_{i=1}^{L} \lambda_i}{\sum_{i=1}^{C-1} \lambda_i} \tag{6}$$

After training process, the eigenvalues corresponding to the first 3 projecting vectors and ACRs when the feature dimension L is set at 1, 2, and 3, are shown in Fig. 10. From the figure, it can be observed that the first 3 projecting vectors can preserve more than 95% of the discriminant information.

The data in different classes points in the 3-dimensional feature space are as shown in Fig. 11. The points of different classes are generally separated visually in the space. From the figure, it can be observed that the samples in F_3 and F_4 classes are near the ones in Nl. Comparatively, the samples in class F_1, F_2 and F_5 are far away from the fault-free samples. In addition, some overlaps between different classes, Nl and F_4 for instance, can also be observed.

Concerning the choice of the dimension of the feature space, on the one hand, more discriminant information can be preserved in a higher dimensional feature space, and on the other hand, the computation cost of performing FDA would increase with the increasing in feature space dimension. In the following section, it can be seen that the computation cost of DAGSVM is also correlated to
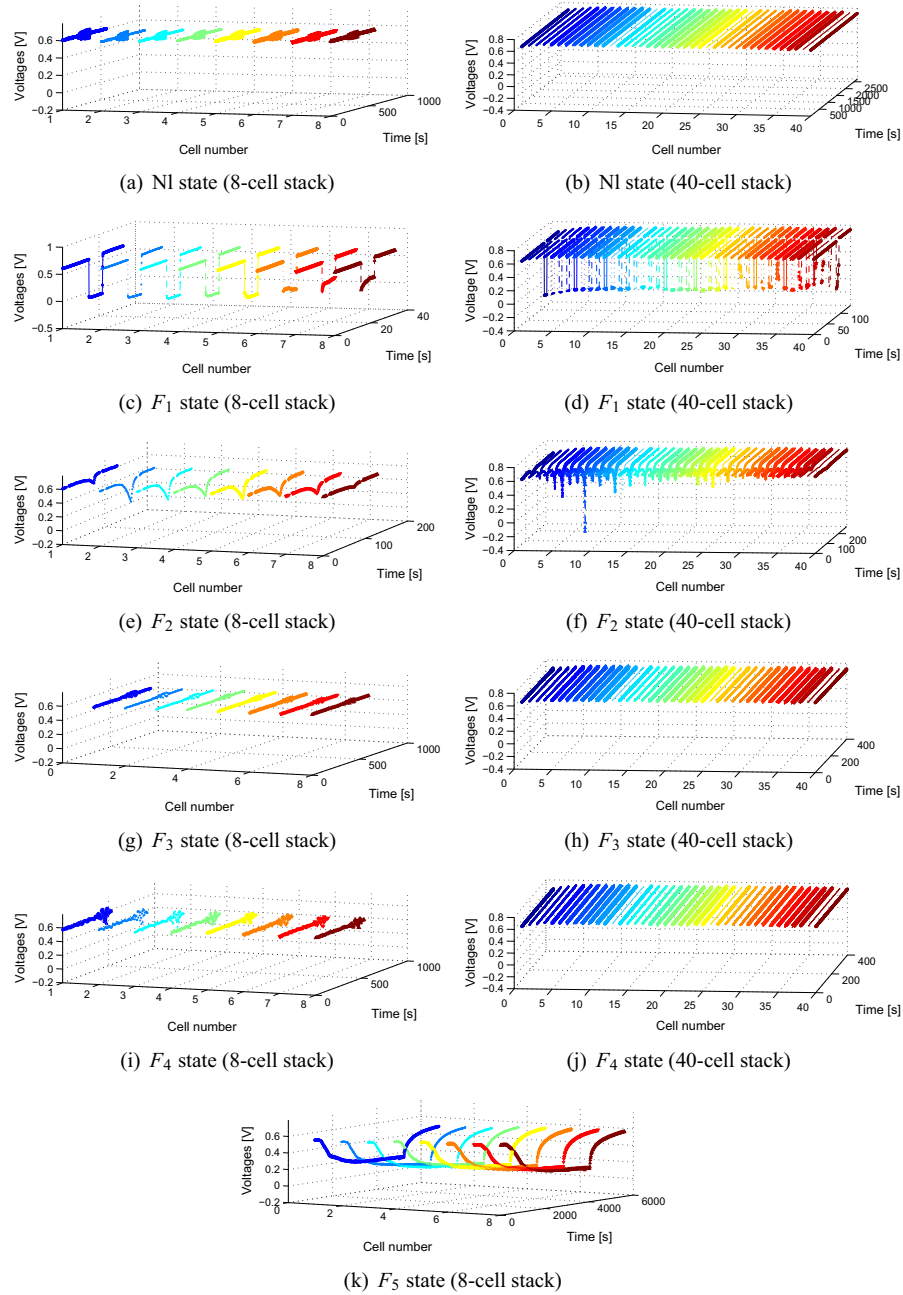
Fig. 9. The evolution of cell voltages in different processes.

Table 4
Sample numbers of the training and test data.

	Nl	F_1	F_2	F_3	F_4	F_5
Training data (8-cell stack)	2474	263	201	253	225	246
Test data (8-cell stack)	3633	239	301	253	180	541
Training data (40-cell stack)	2825	111	21	501	401	Null
Test data (40-cell stack)	5431	31	201	2500	2200	Null

the feature space dimension. Hence, the choice of the feature space dimension must be evaluated with the consideration of the DAGSVM stage.

4.2.2. DAGSVM procedure

After FDA, the DAGSVM classification is carried out to classify the generated features into the relevant classes. To implement

DAGSVM algorithm, parameter σ in (4) and parameter D in (3) were regularized via evaluating the diagnosis accuracy (DA) of the test dataset. After several attempts, the configurations $\sigma = 0.5$ and $D = 1.9 \times 10^4$, with which a relatively higher DA can be obtained, are used to parameter the SVMs.

The performance of the classification procedures in the feature spaces of varied dimension numbers was firstly evaluated. The comparative results for the two stacks are summarized in Tables 5 and 6. From the tables, it can be observed that as the feature dimension number increases, the DAs increase for both training data and test data. This means that the higher classification performance could be obtained in the higher feature space. Apart from that, the number of SVs decreases as the dimension number increases. That is to say, some memory space corresponding SVs and their coefficients could be saved, and the computation could be achieved within a shorter time when DAGSVM is carried out
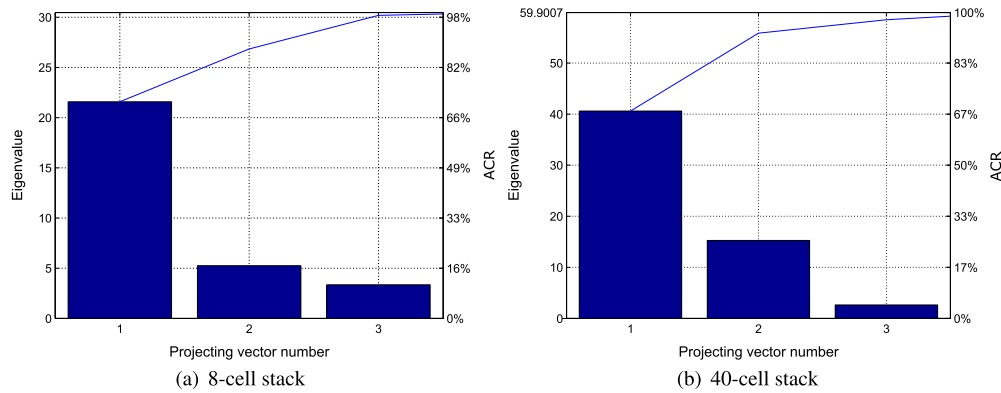
(a) 8-cell stack   (b) 40-cell stack

Fig. 10. Accumulation eigenvalues.

(a) 8-cell stack   (b) 40-cell stack
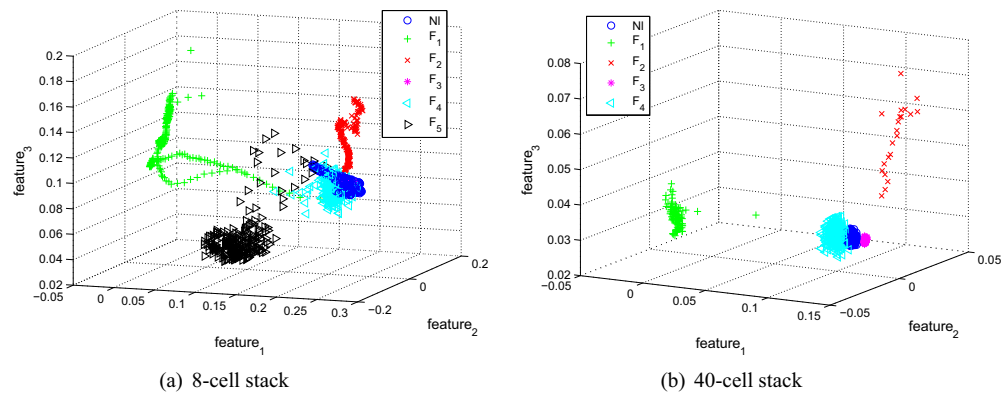
Fig. 11. First three features of the training data sets of 8-cell stack and 40-cell stack.

Table 5
Comparative results of classification in various feature spaces for 8-cell stack.

Dimension number	ACR	DA for training data	DA for test data	Number of SVs
1	0.7082	0.8034	0.8430	1279
2	0.8807	0.9091	0.9172	754
3	0.9908	0.9282	0.9497	660
4	0.9996	0.9869	0.9858	265
5	1	0.9896	0.9885	230

Table 6
Comparative results of classification in various feature spaces for 40-cell stack.

Dimension number	ACR	DA for training data	DA for test data	Number of SVs
1	0.6777	0.8735	0.6270	1150
2	0.9325	0.9978	0.9235	62
3	0.9764	0.9980	0.9331	58
4	1	0.9987	0.9399	54

Table 7
Confusion matrix of the test data for 8-cell stack.

	Diagnosed class					
	Nl	F_1	F_2	F_3	F_4	F_5
Actual class						
Nl	1.0000	0	0	0	0	0
F_1	0	0.9163	0	0	0.0628	0.0209
F_2	0.0399	0	0.9502	0.0100	0	0
F_3	0	0	0	1	0	0
F_4	0.0611	0.0056	0	0.0389	0.8944	0
F_5	0	0	0	0	0.0092	0.9908

Table 8
Confusion matrix of the test data for 40-cell stack.

	Diagnosed class				
	Nl	F_1	F_2	F_3	F_4
Actual class					
Nl	0.9479	0	0	0.0059	0.0462
F_1	0.0323	0.9355	0	0	0.0323
F_2	0	0	1.0000	0	0
F_3	0	0	0	0.9956	0.0044
F_4	0.1486	0	0	0	0.8514

in the higher feature space. Hence, it is recommended to set the feature space dimension number at the maximum possible value (i.e. one less than the class number).

5. Results and discussion

5.1. Diagnosis accuracy

From the above analysis, the DAs of test data for the 8-cell stack and 40-cell stack can be satisfying values when the classification is carried out in a relative high feature dimension (as given in Tables

5 and 6). Other than the global DAs, the mis-classified points should also be analyzed with more attention. The *confusion matrices* of test data sets for the 8-cell stack and the 40-cell stack are summarized in Tables 7 and 8, in which each row represents the diagnosed distribution of the data in an actual class. From the two tables, it can be observed and analyzed that:

Table 9
Comparison with the available approaches.

Used approach	No additional instrumentation	Multi-fault isolation performed	Validated with multiple stacks	Diagnosis accuracy	Computational cost
The present approach (FDA and DAGSVM)	Yes	Yes	Yes	High	Low
PCA [16]	Yes	No	No	Not given	Not given
Neural networks [13]	Yes	No	No	Not given	Not given
Wavelet transformation [14]	Yes	No	No	High	Low
Fuzzy clustering [17]	No	No	No	High	Low
Multifractal analysis [31]	No	No	No	Not given	Low
Bayesian networks [32]	No	No	No	Not given	Low

- For both stacks, the mis-classifications happen mostly on the data of class F_4. The mis-classified points are located mostly in the class of Nl (some are classified to the F_3 class). This means F_4 is a fault type that is the most difficult to detect. For instance, in Table 8, 4.62% points in the Nl class are mis-classified to the F_4 class, and 14.8% samples in the F_4 class appear in the Nl class. It can be inferred that the faults of stoichiometry variation to a certain extent are light faults compared with other types of faults.
- Some mis-classified samples also appear in class F_1, F_2, and F_5. Actually, from our observations, the mis-classification mostly happens at the initial stage of these faults. It could be thought that these samples are located in the transition zone between the normal state and fault state.
- The test data in classes Nl, F_3, and F_4 is from the experiments with EIS tests, which added some current disturbances to the system. With such disturbances, the high classification rates can still be maintained.

The approach is efficient for detecting and isolating the faults whose data are available to train the diagnosis models. Nevertheless, a sample from an unseen failure mode would be mis-classified to one of the known fault classes. Hence, an abundant training dataset, which contains the data from a substantial number of fault classes, is usually necessary for this approach. This is considered as the drawback of the proposed approach.

5.2. Computational costs

In order to implement the proposed diagnosis algorithms online and in an embedded system. The computational costs of the proposed algorithms should be taken into account. Specifically, the occupied memory and online computing time should be evaluated. In our case, when the approach is performed in PC (CPU@2.7 GHz, RAM@8 Go, MATLAB environment), the needed memory is less than 5 kb to save the FDA and SVM models, and the time for perform the approach is less than 0.5 ms. The memory space and computing task can be easily fulfilled. Hence, the approach is suitable for online implementation.

5.3. Comparison with the available approaches

The proposed diagnosis approach is compared with several recently published ones from five perspectives, i.e. whether additional instrumentation is needed, whether the approach is capable of isolating different fault types, whether the approach is validated using multiple PEMFC stacks, the performances of diagnosis accuracy and computational cost. The comparative results are summarized in Table 9. It can be seen that the approach proposed in this study is the only one which is demonstrated to be high-performed in all the five aspects.

6. Conclusion

This article proposes a novel data-driven fault diagnosis approach for PEMFC systems. Only individual cell voltages serve as the original variables for diagnosis. Two methodologies, FDA and DAGSVM, are employed successively to project the raw data into a lower-dimensional feature space and classify the features into the class representing the health state. FDI is achieved consequently.

To validate the FDI performance, five faults involving different components of the PEMFC systems, i.e. the faults of the electric circuit, temperature subsystem, air supply subsystem, and hydrogen supply subsystem, were emulated. The experimental data were collected to train and verify the proposed approach. In our case, it has been found that more accurate diagnosis results can be obtained by performing the classification in a higher-dimensional feature space. Meanwhile, the needed memory and computing time can be decreased. The diagnosis results have shown that the five concerned faults can be detected and isolated with high accuracy. Moreover, the light computation cost (needed memory and computing time) makes the approach suitable as an online diagnosis tool. Additionally, it has been verified that the high diagnosis performance can be maintained with different PEMFC stacks and different fuel cell systems.

At present, the work of coding the approach in an embedded computing chip and online testing is in process. Additionally, to recognize an unseen fault type, some effort is being made to improve the available approach.

Acknowledgment

References

[1] Pei P, Chen H. Main factors affecting the lifetime of proton exchange membrane fuel cells in vehicle applications: a review. Appl Energy 2014;125(0):60–75. http://dx.doi.org/10.1016/j.apenergy.2014.03.048. <http://www.sciencedirect.com/science/article/pii/S0306261914002797>.

[2] DOE hydrogen and fuel cells program: annual report 2012; 2012. <http://www.hydrogen.energy.gov/annual_progress12.html>.

[3] Fuel cell technologies office multi-year research, development and demonstration plan; 2012. <http://www1.eere.energy.gov/hydrogenandfuelcells/mypp/>.

[4] The department of energy hydrogen and fuel cells program plan; 2011. <www.hydrogen.energy.gov/pdfs/program_plan2011.pdf>.

[5] Tian G, Wasterlain S, Endichi I, Candusso D, Harel F, Franois X, et al. Diagnosis methods dedicated to the localisation of failed cells within PEMFC stacks. J Power Sources 2008;182(2):449–61. selected papers from the International Workshop on Degradation Issues in Fuel Cells. http://dx.doi.org/10.1016/j.jpowsour.2007.12.038. <http://www.sciencedirect.com/science/article/pii/S0378775307027061>.

[6] Isermann R. Fault-diagnosis applications. Springer; 2011.

[7] Najafi M, Auslander DM, Bartlett PL, Haves P, Sohn MD. Application of machine learning in the fault diagnostics of air handling units. Appl Energy

2012;96(0):347–58. smart Grids. http://dx.doi.org/10.1016/j.apenergy.2012.02.049. <http://www.sciencedirect.com/science/article/pii/S0306261912001481>.

[8] Bonvini M, Sohn MD, Granderson J, Wetter M, Piette MA. Robust on-line fault detection diagnosis for HVAC components based on nonlinear state estimation techniques. Appl Energy 2014;124(0):156–66. http://dx.doi.org/10.1016/j.apenergy.2014.03.009. <http://www.sciencedirect.com/science/article/pii/S0306261914002311>.

[9] Petrone R, Zheng Z, Hissel D, Pra M, Pianese C, Sorrentino M, et al. A review on model-based diagnosis methodologies for PEMFCs. Int J Hydrogen Energy 2013;38(17):7077–91. http://dx.doi.org/10.1016/j.ijhydene.2013.03.106. <http://www.sciencedirect.com/science/article/pii/S0360319913007465>.

[10] Escobet T, Feroldi D, de Lira S, Puig V, Quevedo J, Riera J, et al. Model-based fault diagnosis in PEM fuel cell systems. J Power Sources 2009;192(1):216–23. http://dx.doi.org/10.1016/j.jpowsour.2008.12.014.

[11] Ding SX. Model-based fault diagnosis techniques: design schemes, algorithms and tools. 2nd ed. Springer; 2013.

[12] Hissel D, Candusso D, Harel F. Fuzzy-clustering durability diagnosis of polymer electrolyte fuel cells dedicated to transportation applications. IEEE Trans Vehicular Technol 2007;56(5):2414–20. http://dx.doi.org/10.1109/TVT.2007.898389.

[13] Yousfi-Steiner N, Hissel D, Moçotéguy P, Candusso D. Diagnosis of polymer electrolyte fuel cells failure modes (flooding & drying out) by neural networks modeling. Int J Hydrogen Energy 2011;36(4):3067–75. http://dx.doi.org/10.1016/j.ijhydene.2010.10.077.

[14] Yousfi-Steiner N, Hissel D, Moçotéguy P, Candusso D. Non intrusive diagnosis of polymer electrolyte fuel cells by wavelet packet transform. Int J Hydrogen Energy 2011;36(1):740–6. http://dx.doi.org/10.1016/j.ijhydene.2010.10.033.

[15] Li Z, Outbib R, Hissel D, Giurgea S. Online diagnosis of PEMFC by analyzing individual cell voltages. In: 2013 European control conference (ECC), Zurich, Switzerland; 2013. p. 2439–44.

[16] Hua J, Lu L, Ouyang M, Li J, Xu L. Proton exchange membrane fuel cell system diagnosis based on the signed directed graph method. J Power Sources 2011;196(14):5881–8. doi:http://dx.doi.org/10.1016/j.jpowsour.2011.03.008.

[17] Zheng Z, Petrone R, Péra M, Hissel D, Becherif M, Pianese C. Diagnosis of a commercial PEM fuel cell stack via incomplete spectra and fuzzy clustering. In: IECON 2013 – 39th annual conference of the IEEE industrial electronics society; 2013. p. 1595–600. http://dx.doi.org/10.1109/IECON.2013.6699371.

[18] Silva RE, Harel F, Jemei S, Gouriveau R, Hissel D, Boulon L, et al. Proton exchange membrane fuel cell operation and degradation in short-circuit. In: 5th International conference on fundamentals & development of fuel cells (FDFC 2013); 2013. p. 1–6.

[19] Candusso D, De Bernardinis A, Péra M-C, Harel F, François X, Hissel D, et al. Fuel cell operation under degraded working modes and study of diode by-pass circuit dedicated to multi-stack association. Energy Convers Manage 2008;49(4):880–95. doi:http://dx.doi.org/10.1016/j.enconman.2007.10.007.

[20] Candusso D, Harel F, De Bernardinis A, François X, Péra M, Hissel D, et al. Characterisation and modelling of a 5 kW PEMFC for transportation applications. Int J Hydrogen Energy 2006;31(8):1019–30. http://dx.doi.org/10.1016/j.ijhydene.2005.11.010. <http://linkinghub.elsevier.com/retrieve/pii/S0360319905003423>.

[21] Duda RO, Hart PE, Stork DG. Pattern classification. Wiley & Sons; 2001.

[22] Fukunaga K. Introduction to statistical pattern recognition. 2nd Edition. Academic Press; 1990.

[23] Cao L, Chua K, Chong W, Lee H, Gu Q, PCA A comparison of. KPCA and ICA for dimensionality reduction in support vector machine. Neurocomputing 2003;55(1):321–36. http://dx.doi.org/10.1016/S0925-2312(03)00433-8.

[24] Platt JC. Sequential minimal optimization: a fast algorithm for training support vector machines. Technical report MSR-TR-98-14, microsoft research; 1998. p. 1–21.

[25] Platt JC, Way M, Shawe-taylor J. Large margin DAGs for multiclass classification. Analysis 2000;12:547–53.

[26] Li Z, Outbib R, Hissel D, Giurgea S. Control engineering practice data-driven diagnosis of PEM fuel cell: a comparative study. Control Eng Pract 2014;28:1–12. http://dx.doi.org/10.1016/j.conengprac.2014.02.019. doi:http://dx.doi.org/10.1016/j.conengprac.2014.02.019.

[27] Hinaje M, Raël S, Caron J-P, Davat B. An innovating application of PEM fuel cell: current source controlled by hydrogen supply. Int J Hydrogen Energy 2012;37(17):12481–8. 12th CHEC. http://dx.doi.org/10.1016/j.ijhydene.2012.05.153. <http://www.sciencedirect.com/science/article/pii/S0360319912013365>.

[28] Giurgea S, Tirnovan R, Hissel D, Outbib R. An analysis of fluidic voltage statistical correlation for a diagnosis of PEM fuel cell flooding. Int J Hydrogen Energy 2013;38(11):4689–96. http://dx.doi.org/10.1016/j.ijhydene.2013.01.060. <http://linkinghub.elsevier.com/retrieve/pii/S0360319913001456>.

[29] Niknezhadi A, Allué-Fantova M, Kunusch C, Ocampo-Martínez C. Design and implementation of LQR/LQG strategies for oxygen stoichiometry control in PEM fuel cells based systems. J Power Sources 2011;196(9):4277–82. http://dx.doi.org/10.1016/j.jpowsour.2010.11.059. <http://linkinghub.elsevier.com/retrieve/pii/S0378775310019658>.

[30] Wagner N, Gülzow E. Change of electrochemical impedance spectra (EIS) with time during CO-poisoning of the Pt-anode in a membrane fuel cell. J Power Sources 2004;127(1–2):341–7. http://dx.doi.org/10.1016/j.jpowsour.2003.09.031. <http://linkinghub.elsevier.com/retrieve/pii/S0378775303009698>.

[31] Benouioua D, Candusso D, Harel F, Oukhellou L. Fuel cell diagnosis method based on multifractal analysis of stack voltage signal. Int J Hydrogen Energy 2014;39(5):2236–45. http://dx.doi.org/10.1016/j.ijhydene.2013.11.066. <http://www.sciencedirect.com/science/article/pii/S0360319913027912>.

[32] Wasterlain S, Candusso D, Harel F, François X, Hissel D. Diagnosis of a fuel cell stack using electrochemical impedance spectroscopy and Bayesian Networks. In: 2010 IEEE vehicle power and propulsion conference (VPPC); 2010. p. 1–6. http://dx.doi.org/10.1109/VPPC.2010.5729184.